Applied Mathematics and Computation 229 (2014) 422–432

Contents lists available at ScienceDirect

Applied Mathematics and Computation

journal homepage: www.elsevier.com/locate/amc

A new phase-field model for a water–oil-surfactant system

Ana Yun [a], Yibao Li [b], Junseok Kim [a,*]

[a] Department of Mathematics, Korea University, Seoul 136-713, Republic of Korea
[b] Department of Computational Science and Engineering, Yonsei University, Seoul 120-749, Republic of Korea

ARTICLE INFO

Keywords:
Surfactant
Interfacial tension
Multiphase flow
Phase-field model
Navier–Stokes equation

ABSTRACT

We propose a new phase-field model to investigate the hydrodynamics of a water–oil-surfactant system. The phase-field method based on the time-dependent Ginzbug–Landau model is developed for the water–oil-surfactant system using two order parameters. We derive the new model in which the water–oil interfacial profile is independent of the surfactant concentration. The proposed model is coupled with the Navier–Stokes equation to have hydrodynamics and it provides an accurate surface tension from the numerical point of view. Various numerical results are presented such as the pressure difference test, calculation of the Dirac-delta function, and the interfacial profile effect to demonstrate the good performance of our model. A droplet deformation under shear flows with Marangoni force is also numerically investigated.

1. Introduction

Water–oil-surfactant mixtures have been widely investigated mainly due to their important applications in everyday life [1–3]. To model these micro-scale mixtures, phase-field models have been studied [1,4] where interfacial transitions of oil–water and surfactant are considered to be infinitely thin interfaces. The dynamics of the water–oil system with surfactants has been investigated by using the time-dependent Ginzburg–Landau (TDGL) free energy functional [5–8] with two order parameters [9–14]. To include the hydrodynamics of the system, the Navier–Stokes (NS) equation is coupled with the water–oil-surfactant system [7,15–18]. The interface motion with fluid flows for immiscible mixtures which has been widely studied [19,20] is described with TDGL–NS system. Surfactants tend to assemble at the water–oil interface and the interfacial surface tension is typically lowered by the presence of surfactants [21]. In the mathematical formulation, the surface tension is represented as a function of surfactants.

However, the straightforward use of the numerical solution for the water–oil-surfactant system can cause unphysical phenomena such as higher interfacial force which leads to higher pressure jump and higher summation of the value of the Dirac-delta function. The main purpose of this paper is to present a robust and accurate phase-field model for solving the water–oil-surfactant system with hydrodynamics. In our model, the water–oil interfacial profile is independent of the surfactant concentration.

The contents are organized as follows: In Section 2, the governing equations are presented with the interfacial tension. In Section 3, a fully discrete semi-implicit finite difference scheme is described. We use a robust nonlinear multigrid method for the phase-field equations and a projection method for the incompressible fluids. Numerical experiments are presented in Section 4. Conclusions are drawn in Section 5.

* Corresponding author.
E-mail address: cfdkim@korea.ac.kr (J. Kim).
URL: http://math.korea.ac.kr/~cfdkim (J. Kim).

0096-3003/$ - see front matter © 2013 Elsevier Inc. All rights reserved.
http://dx.doi.org/10.1016/j.amc.2013.12.054

2. Governing equations

The dynamics of two immiscible fluids and surfactants is modeled by the TDGL free energy functional of the phase-field with two order parameters, ϕ and ψ, which describe the difference in the local densities of the water–oil system and the local concentration of surfactants, respectively [22]. The hydrodynamics is included by using the modified Navier–Stokes equations. The equation for interface advection is replaced by a continuum advective-diffusion equation, where diffusion is driven by chemical potential gradients [23]. Finally, the TDGL–NS system models the hydrodynamics of the water–oil-surfactant system.

2.1. Previous model

We consider a widely used model proposed by van der Sman and van der Graaf [14]:

$$\mathcal{E}(\phi,\psi)=\int_\Omega\left[aF(\phi)+\frac{k}{2}|\nabla\phi|^2-\frac{s\psi}{2}|\nabla\phi|^2+\frac{w}{2}\psi\phi^2+\lambda[\psi\ln\psi+(1-\psi)\ln(1-\psi)]\right]d\mathbf{x}, \tag{1}$$

where the double-well potential $F(\phi)=(\phi^2-1)^2/4$ is the Helmholtz free energy (see Fig. 1). The small positive constant k is the gradient energy coefficient related to the interfacial energy. a, s, w, and λ are positive phenomenological parameters and Ω is a domain. In the free energy functional $\mathcal{E}(\phi,\psi)$, the terms $-0.5s\psi|\nabla\phi|^2$ and $0.5w\psi\phi^2$ prefer a relatively high value of ψ at the water–oil interface. The term $\lambda[\psi\ln\psi+(1-\psi)\ln(1-\psi)]$ restricts the value of ψ to be in the range $(0,1)$.

Let $\mu_\phi=\delta\mathcal{E}/\delta\phi$ and $\mu_\psi=\delta\mathcal{E}/\delta\psi$ be the variational derivatives of the energy functional Eq. (1) with respect to ϕ and ψ. Though the Sman–Graaf [14] includes hydrodynamics with the Lattice Boltzmann equation, let us consider the TDGL–NS system of the Sman–Graaf model as follows:

$$\rho(\mathbf{u}_t+\mathbf{u}\cdot\nabla\mathbf{u})=-\nabla p+\eta\Delta\mathbf{u}+\mathbf{SF}(\phi,\psi), \tag{2}$$

$$\nabla\cdot\mathbf{u}=0, \tag{3}$$

$$\frac{\partial\phi}{\partial t}+\nabla\cdot(\phi\mathbf{u})=M_\phi\Delta\mu_\phi, \tag{4}$$

$$\frac{\partial\psi}{\partial t}+\nabla\cdot(\psi\mathbf{u})=M_\psi\Delta\mu_\psi, \tag{5}$$

$$\mu_\phi=a(\phi^3-\phi)-k\Delta\phi+b\nabla\cdot(\psi\nabla\phi)+c\phi\psi, \tag{6}$$

$$\mu_\psi=-\frac{b}{2}|\nabla\phi|^2+\frac{c}{2}\phi^2+d[\ln\psi-\ln(1-\psi)], \tag{7}$$

where ρ is the density, η is the viscosity, $\mathbf{u}$ is the velocity, p is the pressure, $\mathbf{SF}(\phi,\psi)$ is the interfacial force, M_ϕ and M_ψ are the mobilities of ϕ and ψ, respectively.

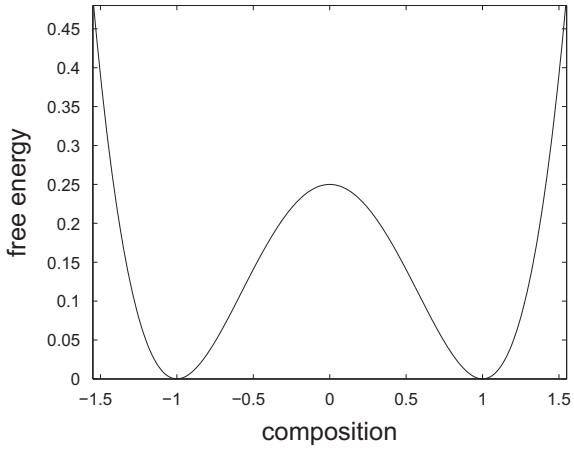

Fig. 1. A double well potential, $(\phi^2-1)^2/4$.

To rewrite the dimensional TDGL–NS system (2)–(7) in dimensionless form, we consider characteristic values: length (L_*), velocity (V_*), viscosity (η_*), density (ρ_*), chemical potentials (μ_{ϕ_*}), (μ_{ψ_*}), and mobilities (M_{ϕ^*}), (M_{ψ^*}). We introduce following non-dimensional variables:

$$\bar{x} = \frac{x}{L_*}, \quad \bar{\mathbf{u}} = \frac{\mathbf{u}}{V_*}, \quad \bar{t} = \frac{tV_*}{L_*}, \quad \bar{p} = \frac{p}{\rho V_*^2}, \quad \bar{\mu}_\phi = \frac{\mu_\phi}{\mu_{\phi_*}}, \quad \bar{\mu}_\psi = \frac{\mu_\psi}{\mu_{\phi_*}},$$

where the bars denote dimensionless variables. After substituting these variables to the governing equations, dropping bar notations, and using the dimensionless numbers, we have the nondimensionalized system:

$$\rho(\mathbf{u}_t + \mathbf{u}\cdot\nabla\mathbf{u}) = -\nabla p + \frac{1}{Re}\Delta\mathbf{u} + \frac{1}{ReCa}\mathbf{SF}(\phi,\psi), \tag{8}$$

$$\nabla\cdot\mathbf{u} = 0, \tag{9}$$

$$\frac{\partial\phi}{\partial t} + \nabla\cdot(\phi\mathbf{u}) = \frac{1}{Pe_\phi}\Delta\mu_\phi, \tag{10}$$

$$\frac{\partial\psi}{\partial t} + \nabla\cdot(\psi\mathbf{u}) = \frac{1}{Pe_\psi}\Delta\mu_\psi, \tag{11}$$

$$\mu_\phi = \phi^3 - \phi - \epsilon^2\Delta\phi + s\nabla\cdot(\psi\nabla\phi) + w\phi,\psi, \tag{12}$$

$$\mu_\psi = -\frac{s}{2}|\nabla\phi|^2 + \frac{w}{2}\phi^2 + \lambda[\ln\psi - \ln(1-\psi)], \tag{13}$$

where $\epsilon = \sqrt{k/(\mu_{\phi_*}L_*^2)}$ is the interfacial thickness for $a = \mu_{\phi_*}$, $s = b/(\mu_{\phi_*}L_*^2)$, $w = c/\mu_{\phi_*}$, $\lambda = d/\mu_{\phi_*}$, $Re = \rho V_* L_*/\eta$ is the Reynolds number which describes the ratio between the inertial force and the viscous force, the Capillary number $Ca = V_*\eta/\sigma_0$, and σ_0 is the surface tension of the clean interface. The diffusional Peclet numbers are $Pe_\phi = L_* V_*/(M_\phi\mu_{\phi_*})$ and $Pe_\psi = L_* V_*/(M_\psi\mu_{\phi_*})$. We let $\rho = 1$ and $\eta = 1$.

The boundary conditions for the TDGL system are zero Neumann boundary conditions

$$v\cdot\nabla\phi = v\cdot\nabla\psi = v\cdot\nabla\mu_\phi = v\cdot\nabla\mu_\psi = 0 \text{ on } \partial\Omega, \tag{14}$$

where v is the outward normal vector to $\partial\Omega$.

2.2. Proposed model

The term $\mathcal{I} = s\nabla\cdot(\psi\nabla\phi) + w\phi\psi$ in Eq. (12) makes the interface of ϕ sharpen and causes unphysical behavior of ϕ. We propose a new model without the term $\mathcal{I}$ as:

$$\rho(\mathbf{u}_t + \mathbf{u}\cdot\nabla\mathbf{u}) = -\nabla p + \frac{1}{Re}\Delta\mathbf{u} + \frac{1}{ReCa}\mathbf{SF}(\phi,\psi), \tag{15}$$

$$\nabla\cdot\mathbf{u} = 0, \tag{16}$$

$$\frac{\partial\phi}{\partial t} + \nabla\cdot(\phi\mathbf{u}) = \frac{1}{Pe_\phi}\Delta\mu_\phi, \tag{17}$$

$$\frac{\partial\psi}{\partial t} + \nabla\cdot(\psi\mathbf{u}) = \frac{1}{Pe_\psi}\Delta\mu_\psi, \tag{18}$$

$$\mu_\phi = \phi^3 - \phi - \epsilon^2\Delta\phi, \tag{19}$$

$$\mu_\psi = -\frac{s}{2}|\nabla\phi|^2 + \frac{w}{2}\phi^2 + \lambda[\ln\psi - \ln(1-\psi)]. \tag{20}$$

Note that the thin interfacial thickness ϵ has the physical value of 3.3×10^{-6} $(\mathrm{J/cm})^{1/2}$ [4] which is difficult to implement with current computational powers. By this reason, an interfacial width for the phase-field model (including the diffuse-interface models) is diffused by the length scale of the numerical spatial step size [19].

Interfacial force $\mathbf{SF}(\phi,\psi)$ satisfying the Laplace–Young condition is given as the summation of the interfacial surface tension and Marangoni force [8,24,25]:

$$\mathbf{SF}(\phi,\psi) = -\sigma(\psi)\kappa\delta\mathbf{n} + \delta(\nabla_s\sigma(\psi)) = -\sigma(\psi)(\nabla\cdot\mathbf{n})\alpha\epsilon|\nabla\phi|^2\mathbf{n} + \alpha\epsilon|\nabla\phi|^2[(\mathbf{I} - \mathbf{n}\otimes\mathbf{n})\nabla\sigma(\psi)],$$

where $\sigma(\psi)$ is the interfacial tension depending on the surfactant concentration, $\delta = \alpha\epsilon|\nabla\phi|^2$ is a smoothed Dirac-delta distribution and $\alpha = 3\sqrt{2}/4$ [26], $\mathbf{n} = \nabla\phi/|\nabla\phi|$ is the unit normal vector to the interface of two immiscible phases, $\kappa = \nabla\cdot(\nabla\phi/|\nabla\phi|)$ is the mean curvature, and $\nabla_s = (\mathbf{I} - \mathbf{n}\otimes\mathbf{n})\nabla$ is the surface gradient operator. Note that the smoothed Dirac-delta distribution in interfacial force only depends on ϕ. Therefore, even though surfactant changes interfacial force, it does not alter the distribution of ϕ. The nonlinear dependence of the interfacial tension $\sigma(\psi)$ is given through a constitutive law as

$$\sigma(\psi) = \sigma_0 + RT\psi_\infty \ln\left(1 - \frac{\psi}{\psi_\infty}\right), \tag{21}$$

where σ_0 is the surface tension of the clean interface, R is the gas constant, T is the temperature, and ψ_∞ denotes the monolayer saturation concentration (scaled by the initial equilibrium concentration), which is a theoretical limit [27,28]. Let $\beta = RT\psi_\infty/\sigma_0$, then we have a nondimensionalized $\sigma(\psi)$

$$\sigma(\psi) = 1 + \beta \ln\left(1 - \frac{\psi}{\psi_\infty}\right), \tag{22}$$

where the elasticity number β is a measure of the sensitivity of interfacial tension to variations in the surfactant concentration.

Note that Eq. (22) is a form of the Langmuir equation of state [29], in which we assume that there are no adhesive or repulsive interactions between the surfactant molecules. The term has been widely used in studying the fluid-surfactant dynamics [6,8,11,27,29]. In [5,14,21], the authors use the interfacial force from the Gibbs–Duhem equality where the excess chemical potential gradients give rise to a thermodynamic force as

$$\mathbf{SF}(\phi,\psi) = -\phi\nabla\mu_\phi - \psi\nabla\mu_\psi. \tag{23}$$

The main differences between the proposed model and the Sman–Graaf model are that (1) the present model omits the interface sharpening term $\mathcal{I}$; (2) the present model uses the Navier–Stokes equation, whereas the Sman–Graaf model uses the Lattice Boltzmann equation; and (3) the present model uses the interface force from geometric feature of surface, whereas the Sman–Graaf model uses a formulae from the thermodynamics. (see Fig. 2)

3. Numerical solution

We present the algorithm for numerical solution on a staggered grid [30]. ϕ, ψ, and p are defined at the cell center. Each velocity component u and v from velocity $\mathbf{u} = (u, v)$ is defined at vertical lines and horizontal lines (see Fig. 3).

Let us discretize Eqs. (15)–(20) in two-dimensional space $\Omega = (a,b)\times(c,d)$. Let N_x and N_y be the numbers of cells in x- and y-directions, respectively. Then, $h = (b-a)/N_x = (d-c)/N_y$ be the uniform mesh size. Let $\Omega_{ij} = \{(x_i, y_j) : x_i = a + (i-0.5)h, y_j = c + (j-0.5)h, 1 \leqslant i \leqslant N_x, 1 \leqslant j \leqslant N_y\}$ be the set of cell-centers. The cell vertices are $(x_{i+\frac{1}{2}}, y_{j+\frac{1}{2}}) = (ih, jh)$. Velocity components u and v are located at $(x_{i+\frac{1}{2}}, y_j)$, $(x_i, y_{j+\frac{1}{2}})$, respectively. Let ϕ^n_{ij} be approximations of $\phi(x_i, y_j, n\Delta t)$, where Δt is the time step. We implement the zero Neumann boundary condition (14) by requiring that

$$\phi^n_{0j} = \phi^n_{1j}, \phi^n_{N_x+1,j} = \phi^n_{N_xj}, \quad \phi^n_{i0} = \phi^n_{i1}, \phi^n_{i,N_y+1} = \phi^n_{iN_y}, \tag{24}$$

for $j = 1,\ldots,N_y$ and $i = 1,\ldots,N_x$. The discrete differentiation operators are given as

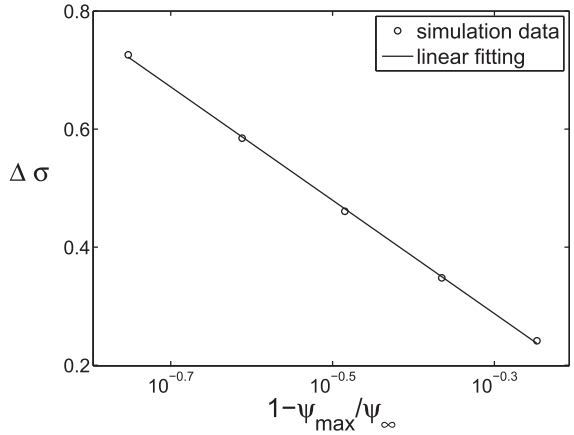

Fig. 2. Semilogarithmic plot of $\Delta\sigma$ against $1 - \psi_{max}/\psi_\infty$. Results obtained by simulation (represented with circles) and linear fitting (represented with solid line).

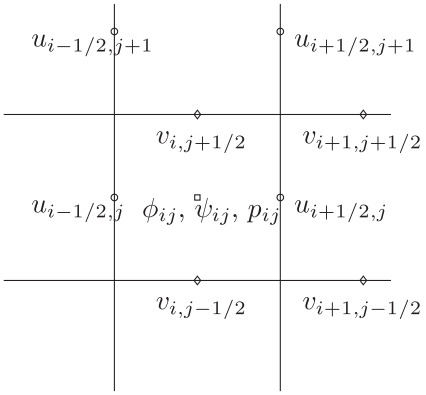

Fig. 3. ϕ, ψ, and p are defined at the cell center. u and v are defined at the cell edges.

$$D_x\phi_{i+1/2,j} = \frac{\phi_{i+1,j} - \phi_{ij}}{h}, \quad D_y\phi_{i,j+1/2} = \frac{\phi_{i,j+1} - \phi_{ij}}{h},$$

$$\nabla \cdot \phi_{ij} = D_x\phi_{ij} + D_y\phi_{ij},$$

$$\nabla\phi_{ij} = \left(D_x\phi_{i+1/2,j}, D_y\phi_{i,j+1/2}\right),$$

$$\nabla^c\phi_{ij} = \left(\frac{D_x\phi_{i+1/2,j} + D_x\phi_{i-1/2,j}}{2}, \frac{D_y\phi_{ij+1/2} + D_y\phi_{ij-1/2}}{2}\right),$$

$$\Delta\phi_{ij} = \frac{D_x\phi_{i+1/2,j} - D_x\phi_{i-1/2,j} + D_y\phi_{ij+1/2} - D_y\phi_{ij-1/2}}{h}.$$

Then, a semi-implicit time and centered difference space discretization of Eqs. (15)–(20) is given by

$$\frac{\mathbf{u}^{n+1} - \mathbf{u}^n}{\Delta t} = -\nabla p^{n+1} + \frac{1}{Re}\Delta\mathbf{u}^n + \frac{1}{ReCa}\mathbf{SF}^n - (\mathbf{u}\cdot\nabla\mathbf{u})^n, \tag{25}$$

$$\nabla \cdot \mathbf{u}^{n+1} = 0, \tag{26}$$

$$\frac{\phi^{n+1} - \phi^n}{\Delta t} = \frac{1}{Pe_\phi}\Delta\mu_\phi^{n+1} - \nabla\cdot(\phi\mathbf{u})^n, \tag{27}$$

$$\mu_\phi^{n+1} = \left(\phi^{n+1}\right)^3 - \phi^n - \epsilon^2\Delta\phi^{n+1}, \tag{28}$$

$$\frac{\psi^{n+1} - \psi^n}{\Delta t} = \frac{1}{Pe_\psi}\Delta\mu_\psi^{n+1} - \nabla\cdot(\psi\mathbf{u})^n, \tag{29}$$

$$\mu_\psi^{n+1} = -\frac{s}{2}|\nabla^c\phi^{n+1}|^2 + \frac{w}{2}\left(\phi^{n+1}\right)^2 + \lambda[\ln\psi^n - \ln(1-\psi^n)]. \tag{30}$$

The one time step is proceeded as follows.

Step 1. Solve the Navier–Stokes Eqs. (25) and (26) on the rectangular grid to get $\mathbf{u}^{n+1}$ and p^{n+1} from $\mathbf{u}^n$ and $\mathbf{SF}^n$ by employing the projection method [31].
Let us discretize $\mathbf{SF}^n$. The normal vector at the top right vertex of cell (i,j) is given by

$$\mathbf{m}_{i+\frac{1}{2}j+\frac{1}{2}} = \left(m^x_{i+\frac{1}{2}j+\frac{1}{2}}, m^y_{i+\frac{1}{2}j+\frac{1}{2}}\right) = \left(\frac{\phi_{i+1,j} + \phi_{i+1,j+1} - \phi_{ij} - \phi_{i,j+1}}{2h}, \frac{\phi_{i,j+1} + \phi_{i+1,j+1} - \phi_{ij} - \phi_{i+1,j}}{2h}\right).$$

The other normal vectors are defined in the same manner. Then the curvature at the cell center is

$$\nabla^e \cdot \left(\frac{\mathbf{m}}{|\mathbf{m}|}\right)_{ij} = \frac{1}{2h}\left(\frac{m^x_{i+\frac{1}{2}j+\frac{1}{2}} + m^y_{i+\frac{1}{2}j+\frac{1}{2}}}{|\mathbf{m}_{i+\frac{1}{2}j+\frac{1}{2}}|} + \frac{m^x_{i+\frac{1}{2}j-\frac{1}{2}} - m^y_{i+\frac{1}{2}j-\frac{1}{2}}}{|\mathbf{m}_{i+\frac{1}{2}j-\frac{1}{2}}|} - \frac{m^x_{i-\frac{1}{2}j+\frac{1}{2}} - m^y_{i-\frac{1}{2}j+\frac{1}{2}}}{|\mathbf{m}_{i-\frac{1}{2}j+\frac{1}{2}}|} - \frac{m^x_{i-\frac{1}{2}j-\frac{1}{2}} + m^y_{i-\frac{1}{2}j-\frac{1}{2}}}{|\mathbf{m}_{i-\frac{1}{2}j-\frac{1}{2}}|}\right).$$

The cell-centered normal is the average of vertex normals,

$$\nabla^e \phi_{ij} = \left(\mathbf{m}_{i+\frac{1}{2}j+\frac{1}{2}} + \mathbf{m}_{i+\frac{1}{2}j-\frac{1}{2}} + \mathbf{m}_{i-\frac{1}{2}j+\frac{1}{2}} + \mathbf{m}_{i-\frac{1}{2}j-\frac{1}{2}}\right)/4.$$

The unit normal vector, $\mathbf{n}_{ij} = (n^x_{ij}, n^y_{ij})$, is defined as $\nabla^e\phi_{ij}/|\nabla^e\phi_{ij}|$. Then the surface tension force **SF** is discretized as

$$\begin{aligned}\mathbf{SF}(\phi_{ij},\psi_{ij}) &= -\sigma(\psi_{ij})\alpha\epsilon\nabla^e \cdot \left(\frac{\mathbf{m}}{|\mathbf{m}|}\right)_{ij} |\nabla^e\phi_{ij}|\nabla^e\phi_{ij} + \alpha\epsilon(\mathbf{I} - \mathbf{n}\otimes\mathbf{n})_{ij}\nabla\sigma(\psi_{ij})|\nabla^e\phi_{ij}|^2 \\ &= -\sigma(\psi_{ij})\alpha\epsilon\nabla^e \cdot \left(\frac{\mathbf{m}}{|\mathbf{m}|}\right)_{ij} |\nabla^e\phi_{ij}|\nabla^e\phi_{ij} \\ &\quad + \alpha\epsilon\Big((1-(n^x_{ij})^2)D_x\sigma(\psi_{ij}) - n^x_{ij}(n^y_{ij})^2 D_y\sigma(\psi_{ij}), -n^x_{ij}n^y_{ij}D_x\sigma(\psi_{ij}) + (1-(n^y_{ij})^2)D_y\sigma(\psi_{ij})\Big)|\nabla^e\phi_{ij}|^2.\end{aligned}$$

We decompose Eq. (25) into two steps. First, we solve an intermediate velocity field $\tilde{\mathbf{u}}$ without the pressure gradient term,

$$\frac{\tilde{\mathbf{u}} - \mathbf{u}^n}{\Delta t} = \frac{1}{Re}\Delta\mathbf{u}^n + \frac{1}{ReCa}\mathbf{SF}^n - (\mathbf{u}\cdot\nabla\mathbf{u})^n. \tag{31}$$

Second, we solve the following equations for the pressure field at $(n+1)$ time step.

$$\frac{\mathbf{u}^{n+1} - \tilde{\mathbf{u}}}{\Delta t} = -\nabla p^{n+1}, \tag{32}$$

$$\nabla\cdot\mathbf{u}^{n+1} = 0. \tag{33}$$

Taking the discrete divergence operator to Eq. (32) and using Eq. (33), we have the Poisson equation for the pressure at the time $(n+1)$, which is solved using a multigrid method.

$$\Delta p^{n+1} = \frac{1}{\Delta t}\nabla\cdot\tilde{\mathbf{u}}. \tag{34}$$

Then the divergence-free velocities u^{n+1} and v^{n+1} are defined by

$$\mathbf{u}^{n+1} = \tilde{\mathbf{u}} - \Delta t\nabla p^{n+1}. \tag{35}$$

Step 2. Update the composition fields ϕ^n and ψ^n to ϕ^{n+1} and ψ^{n+1} from Eqs. 27,28,29,30. Here $\nabla\cdot(\phi\mathbf{u})^n$ is computed in a conservative form such as

$$\nabla\cdot(\phi\mathbf{u})^n_{ij} = \frac{u^n_{i+\frac{1}{2}j}(\phi^n_{i+1j} + \phi^n_{ij}) - u^n_{i-\frac{1}{2}j}(\phi^n_{ij} + \phi^n_{i-1j})}{2h} + \frac{v^n_{ij+\frac{1}{2}}(\phi^n_{ij+1} + \phi^n_{ij}) - v^n_{ij-\frac{1}{2}}(\phi^n_{ij} + \phi^n_{ij-1})}{2h}.$$

We apply an unconditionally gradient stable type scheme and use a nonlinear multigrid solver [32] to solve Eqs. (27)–(30). For a detailed description of the numerical method used in solving these equations, please refer to [33,34]. These steps complete one time step.

4. Numerical experiments

To show the accuracy of the proposed model, we perform numerical experiments such as pressure jump, effect of the term $\mathcal{I}$, calculation of the Dirac-delta function, and droplet deformation. Here we define the numerical steady state when the l_2 norm between ψ^{n+1} and ψ^n becomes less than a tolerance, i.e., $||\psi^{n+1} - \psi^n||_2 = \sqrt{\sum_{i=1}^{N_x}\sum_{j=1}^{N_y}(\psi^{n+1}_{ij} - \psi^n_{ij})^2/(N_xN_y)} < 10^{-6}$. Unless otherwise specified, we use $\psi(x,y,0) = \psi_{avarge} = 0.2$, $\lambda = 0.02$, $\beta = 0.5$, and $\psi_\infty = 1$. For the numerical experiments, we focus on investigating the hydrodynamics in which surfactant concentration is relatively high. It should be noted that if surfactant concentration is relatively small, then the value of the term $\mathcal{I}$ approaches to zero and our proposed model shows similar results to the van der Sman and van der Graaf model [14]. Also note that the Engblom et al.'s model [5], in which they replaced $-s\psi|\nabla\phi|^2$ by $-s\psi(1-\phi^2)^2/(4\epsilon^2)$ to produce a sharper equilibrium profile.

4.1. Pressure difference

We calculate the pressure difference $[p]$ to compare the analytical prediction with the numerical solution of our proposed model. In this numerical test, we calculate the governing equations (15)–(17), (19) with the initial condition

Table 1
Error with mesh refinement.

Mesh sizes	64×64	128×128	256×256	512×512
Relative error	0.2568	0.0856	0.0269	0.0098

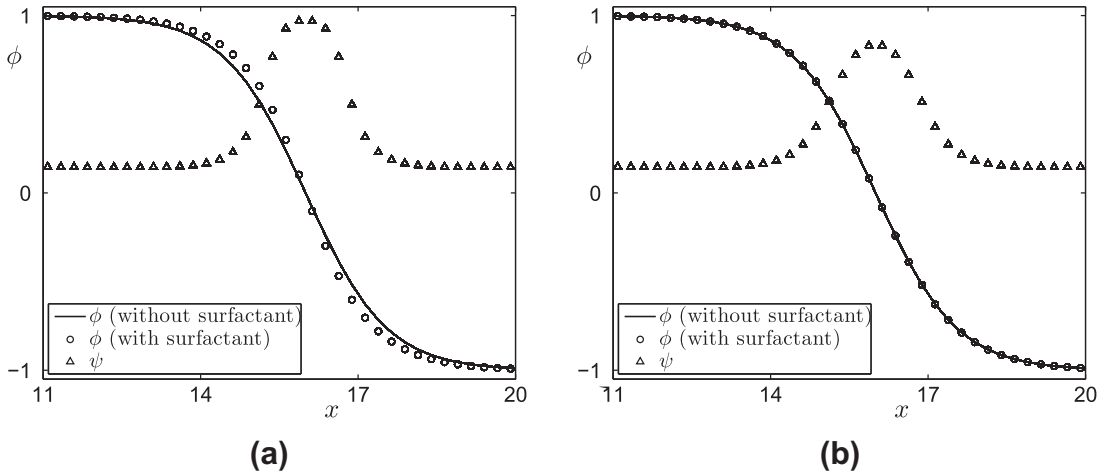

Fig. 4. Overlapped numerical solutions of the order parameter ϕ and the surfactant concentration ψ (a) with and (b) without $\mathcal{I}$ at the steady state. For comparison, we also plot the equilibrium profile of ϕ without surfactant.

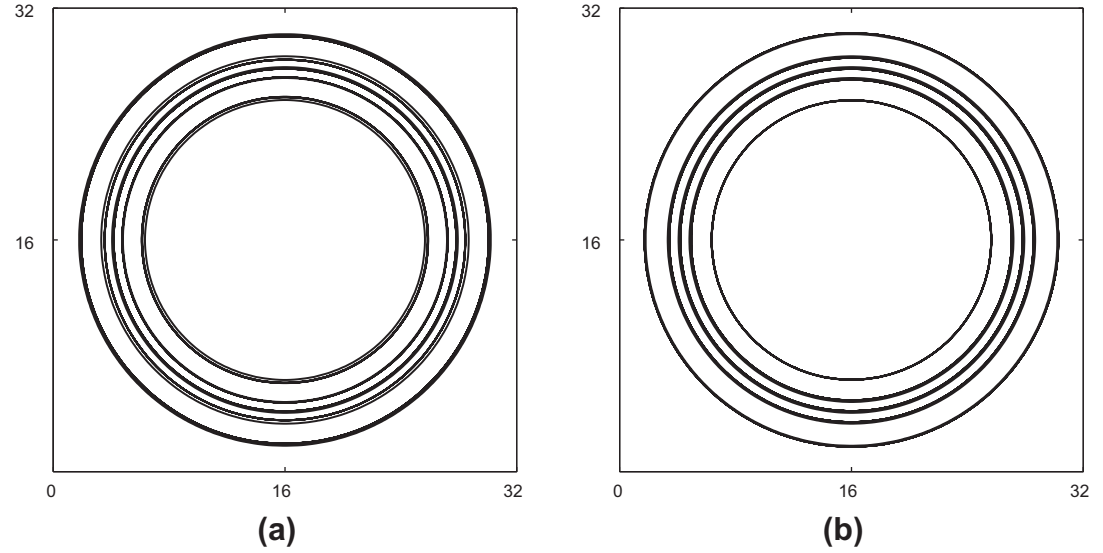

Fig. 5. Contour plots of order parameter ϕ at four levels (a) with and (b) without $\mathcal{I}$ at the steady state. Note that we overlap the steady state of a clean droplet for comparison.

$\phi(x, y, 0) = \tanh[(0.4 - \sqrt{(x-0.5)^2 + (y-0.5)^2})/(\sqrt{2}\epsilon)]$ on the unit domain $(0,1) \times (0,1)$. The pressure jump across interface for a clean droplet with a radius $r = 0.4$ is analytically given by the Laplace law $[p]_{\text{exact}} = 1/(rReCa)$ [35]. Parameters $\epsilon = 0.01$, $Re = 100$, $Ca = 0.01$, and $Pe_\phi = 1$ are used. With finer mesh sizes up to four levels such as 64×64, 128×128, 256×256, and 512×512, we compute the relative error, $|[p]_{\text{exact}} - [p]_{\text{numerical}}|/[p]_{\text{exact}}$. Table 1 shows that the numerical pressure difference approaches to the analytic value with mesh refinements.

If there is surfactant around the droplet, then the interfacial tension $\sigma(\psi)$ depends on surfactant concentration: $\sigma(\psi) = 1 + \beta \ln(1 - \psi/\psi_\infty)$. Fig. 2 shows the semilogarithmic plot of $\Delta\sigma = 1 - \sigma(\psi_{max})$ against $1 - \psi_{max}/\psi_\infty$, where ψ_{max} is

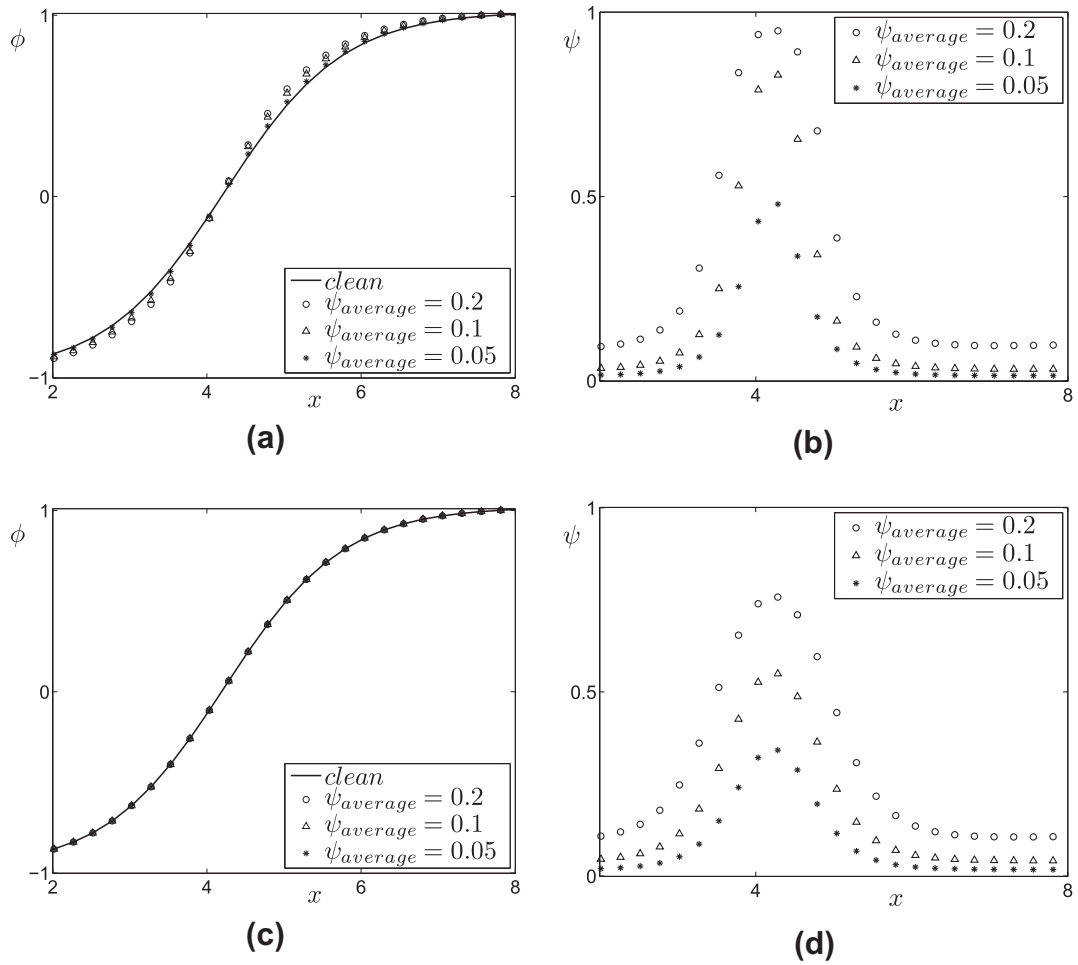

Fig. 6. Plots of ϕ and ψ at $y = 16$ with various surfactant concentrations: (a) ϕ and (b) ψ with $\mathcal{I}$; (c) ϕ and (d) ψ without $\mathcal{I}$.

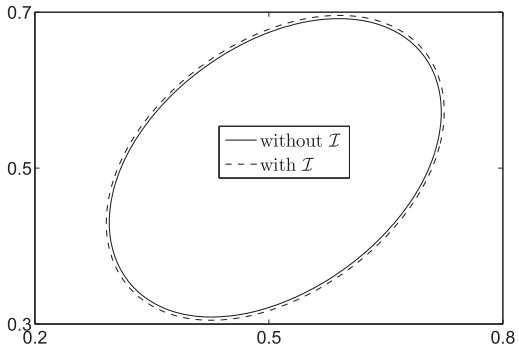

Fig. 7. Droplet profiles with (dashed line) and without (solid line) the term $\mathcal{I}$.

the maximum value of surfactant concentration in equilibrium condition and $\sigma(\psi_{max}) = rReCa[p]$ is calculated numerically. Here we used several different average surfactant concentrations $\psi_{avarage} = 0.2, 0.3, 0.4, 0.5, 0.6$ and $\beta = 0.5$, $\psi_\infty = 1$. We expect the relation $\sigma(\psi_{max}) - 1 \sim \ln(1 - \psi_{max}/\psi_\infty)$ by the equation of state and Fig. 2 demonstrates that our numerical results (represented with circles) fit well to the linear fitting (represented with solid line).

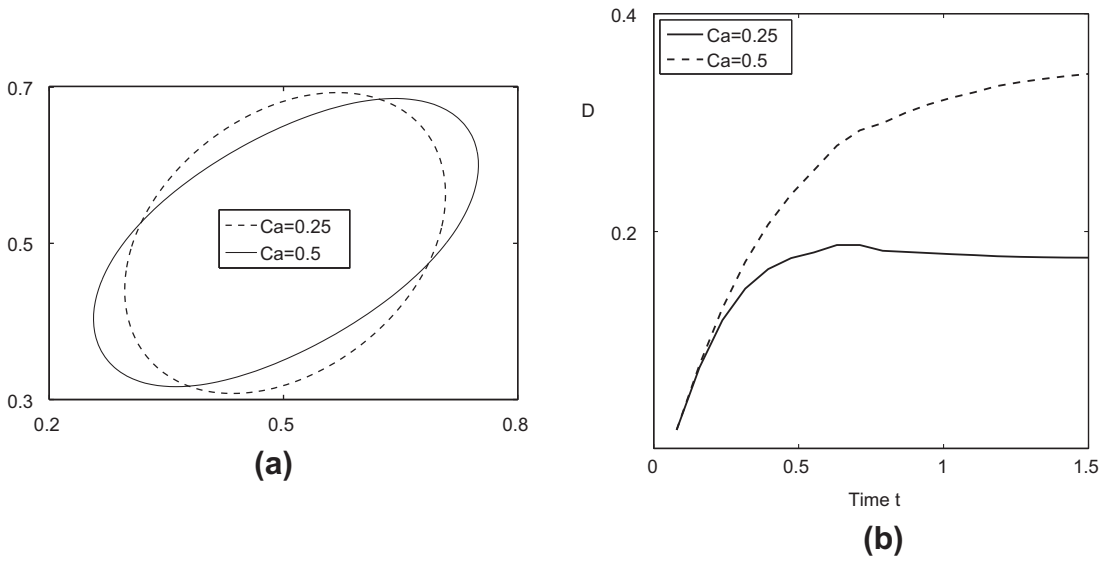

Fig. 8. Effect of Ca number: (a) contour plots of ϕ and (b) deformation rate with $Ca = 0.25$ (dashed line) and $Ca = 0.5$ (solid line).

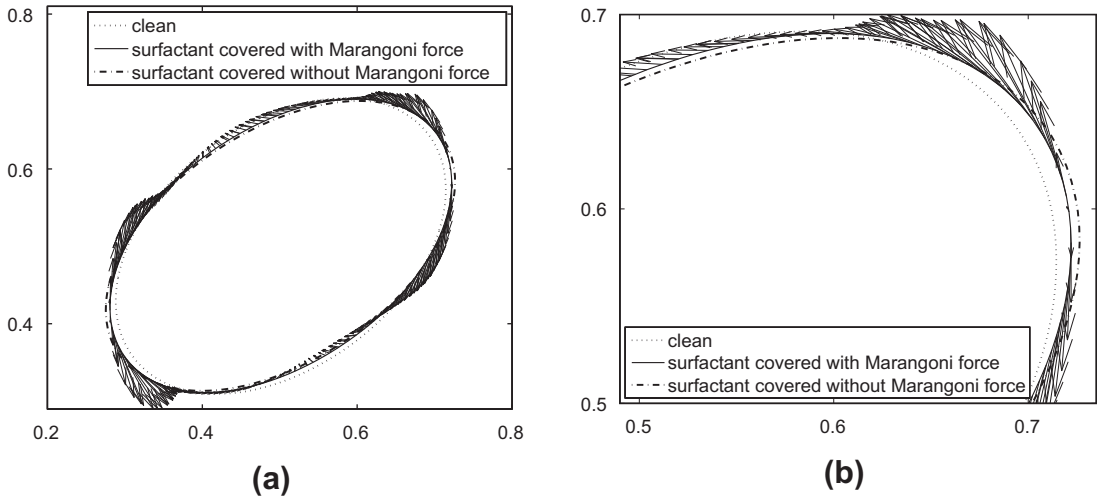

Fig. 9. Contour lines droplet with clean, surfactant with Marangoni force, and surfactant without Marangoni force (a) and its close-up view (b). The arrows are the Marangoni stress vector field along the interface of the droplet.

4.2. Interface sharpening effect and Dirac-delta function

With Eqs. (10)–(13), we investigate the effect of the interface sharpening term $\mathcal{I}$ on the interfacial profile with high surfactant concentration without flow. Here, the initial condition is given as $\phi(x, y, 0) = \tanh[(16 - x)/(\sqrt{2}\epsilon)]$ on the domain $\Omega = (0, 32) \times (0, 32)$. The parameter values $\epsilon = 18h/(2\sqrt{2}\tanh^{-1}(0.9))$, $s = 0.3\epsilon$, $w = 0.0001$, $Pe_\phi = 1$, and $Pe_\psi = 50$ are used with a time step $\Delta t = 0.4$ and a space step $h = 0.25$. Fig. 4(a) and (b) show the order parameter ϕ and the surfactant concentration ψ on $y = 16$ with and without $\mathcal{I}$, respectively. To compare numerical results with and without surfactant, we overlap the equilibrium profiles. As can be seen that the interfacial transition of the order parameter ϕ becomes sharper when the term $\mathcal{I}$ is included. However, without the term $\mathcal{I}$, ϕ does not change. In both cases, surfactant has relatively high concentration at the interfacial region of ϕ.

Across the interface, $\alpha\epsilon\sum_{i=1}^{N_x}(D_x\phi_{i+1/2,Ny/2})^2 h$, the summation of the smoothed Dirac-delta function, should equal to 1. With and without $\mathcal{I}$, the values are 1.1809 and 0.9955, respectively. This result suggests that we have a better smoothed Dirac-delta function without the term $\mathcal{I}$.

Next, we consider a droplet which is placed on the center of computational domain $(0,32)\times(0,32)$ with a radius of 12. The initial condition is $\phi(x,y,0)=\tanh\left[\left(12-\sqrt{(x-16)^2+(y-16)^2}\right)/(\sqrt{2}\epsilon)\right]$. Here we use $Pe_\phi=10$, $Pe_\psi=50$, $\epsilon=18h/[2\sqrt{2}\tanh^{-1}(0.9)]$, $s=0.3\epsilon$, $h=0.25$, and $\Delta t=0.4$. Overlapped contour plots of the order parameter ϕ at four levels from -1 to 1 (a) with and (b) without $\mathcal{I}$ at the steady state are shown in Fig. 5. Here we overlap the interface of clean droplet for comparison. With the term $\mathcal{I}$, (a), interface ϕ is shrinked than the clean droplet. However, without the term, (b), we observe the interface of ϕ is exactly the same as the clean droplet. Then we consider various surfactant concentrations such as $\psi_{average}=0.2$(represented with circles), 0.1(represented with triangles), and 0.05(represented with stars) for a droplet in Fig. 5. Fig. 6(a) and (b) show ϕ and ψ with $\mathcal{I}$ at $y=16$ plane, respectively. In (a), we overlap steady state of the clean droplet (represented with solid line) for comparison. The interface sharpening phenomenon diminishes when the value of the bulk concentration of surfactant is small. Fig. 6(c) and (d) show ϕ and ψ without $\mathcal{I}$ at $y=16$ plane, respectively. In (c), steady state of the clean droplet (represented with solid line) is completely overlapped to the steady states with surfactant. We deduce that the profile of ϕ is independent of the amount of surfactant concentration.

4.3. Deformation of a droplet under shear flow

We investigate the effect of the term $\mathcal{I}$ on the deformation of a droplet under a simple shear flow. We consider a drop of radius $r=0.2$ on $\Omega=(0,1)\times(0,1)$, i.e., $\phi(x,y,0)=\tanh[(0.2-\sqrt{(x-0.5)^2+(y-0.5)^2})/(\sqrt{2}\epsilon))]$. The TDGL–NS system is solved with a spatial mesh size 128×128 and a temporal step $\Delta t=2h^2$ up to time $T=2.44$. We impose a shear flow with the top and bottom lid moving in opposite directions. In this simulation we take the parameters: $Re=10$, $Ca=0.3$, $\epsilon=0.015$, $s=0.00002$, $Pe_\phi=100$, $Pe_\psi=100$, and $w=0.00002$. Fig. 7 shows the contour lines of the droplet ϕ with (dashed line) and without (solid line) the term $\mathcal{I}$. In the case of without the term $\mathcal{I}$, the droplet ends are more elongated than that of with the term. This is due to the higher surface tension effect from the sharp interface profile with $\mathcal{I}$.

Then we investigate the effect of Capillary number on the deformation of the droplet. Let the Taylor deformation parameter be $D=(L-B)/(L+B)$, where L and B are the maximum and the minimum distances of the drop interface from its center, respectively. Fig. 8(a) and (b) show the droplet shapes and the Taylor deformation parameter D with $Ca=0.25$ (dashed line) and $Ca=0.5$ (solid line) at $T=1.5$, respectively. The parameters $Re=10$, $Pe_\phi=0.1$, $Pe_\psi=2$, $\epsilon=0.015$, $s=0.00001$, and $w=0.00001$ are used. This result illustrates that the bigger value of Ca makes more elongated droplet.

4.4. Effect of Marangoni stress term on a droplet under a shear flow

Finally, we study the effect of the Marangoni force on the droplet deformation under a shear flow. The parameters are the same as Section 4.3. Fig. 9 shows the contour lines droplet with clean, surfactant with Marangoni force, and surfactant without Marangoni force (a) and its close-up view (b). Here we overlap the Marangoni stress vector field along the interface of the droplet. From the results, we deduce that surfactants lower the interfacial tension and promote drop deformation. Meanwhile, the Marangoni stress retards the convective flux and opposes the interfacial velocity.

5. Conclusions

We have proposed a new phase-field model to investigate the hydrodynamics of a water–oil-surfactant system. The new model has a good numerical property that the water–oil profile is independent of the surfactant concentrations. With our model, an accurate interfacial tension was provided, which resulted in an appropriate calculation of the surface force. We used a nonlinear multigrid method for the phase-fields and a projection method for the incompressible Navier–Stokes equations. To show the accuracy of our proposed model, the pressure jump was calculated. We compared numerical results of previous and proposed models for pressure difference, calculation of the Dirac-delta function and the interfacial profiles for the equilibrium states. Numerical experiments for a droplet under shear flows with Marangoni force were included. Overall, our proposed model showed good performance compared to the previous approaches.

Acknowledgments

The first author (A. Yun) was supported by National Junior research fellowship from the National Research Foundation of Korea Grant funded by the Korea government (No. 2011-00012258). The corresponding author (J.S. Kim) is grateful to the anonymous referees whose valuable suggestions and comments significantly improved the quality of this paper.

References

[1] G. Gompper, S. Zschocke, Ginzburg–Landau theory of oil–water-surfactant mixtures, Phys. Rev. A 46 (1992) 4836–4851.
[2] T. Hargreaves, Chemical Formulation: An Overview of Surfactant-Based Preparations Used in Everyday Life, Royal Society of Chemistry, Cambridge, UK, 2003.

[3] R.J.W. Meesters, H.F. Schröder, Perfluorooctane sulfonate: a quite mobile anionic anthropogenic surfactant, ubiquitously found in the environment, Water Sci. Technol. 50 (2004) 235–242.
[4] A.A. Wheeler, W.S. Boettinger, G.B. McFadden, Phase-field model for isothermal phase transitions in binary alloys, Phys. Rev. A 45 (1992) 7424–7440.
[5] S. Engblom, M. Do-Quang, G. Amberg, A.-K. Tornberg, On diffuse interface modeling and simulation of surfactants in two-phase fluid flow, Commun. Comput. Phys. 14 (2013) 879–915.
[6] M.-C. Lai, Y.-H. Tseng, H. Huang, An immersed boundary method for interfacial flows with insoluble surfactant, J. Comput. Phys. 227 (2008) 7279–7293.
[7] G. Pätzold, K. Dawson, Numerical simulation of phase separation in the presence of surfactants and hydrodynamics, Phys. Rev. E 52 (1995) 6908–6911.
[8] K.E. Teigen, P. Song, J. Lowengrub, A. Voigt, A diffuse-interface method for two-phase flows with soluble surfactants, J. Comput. Phys. 230 (2011) 375–393.
[9] M. Laradji, H. Guo, M. Grant, M.J. Zuckermann, The effect of surfactants on the dynamics of phase separation, J. Phys. Condens. Matter 4 (1992) 6715–6728.
[10] Y. Li, J.S. Kim, A comparison study of phase-field models for an immiscible binary mixture with surfactant, Eur. Phys. J. B 85 (2012) 1–9.
[11] C.-H. Teng, I.-L. Chern, M.-C. Lai, Simulating binary fluid-surfactant dynamics by a phase field model, Discrete Contin. Dyn. Syst. B 4 (17) (2012) 1289–1307.
[12] T. Teramoto, F. Yonezawa, Droplet growth dynamics in a water/oil/surfactant system, J. Colloid Interface Sci. 235 (2001) 329–333.
[13] O. Theissen, G. Gompper, Lattice-Boltzmann study of spontaneous emulsification, Eur. Phys. J. B 11 (1) (1999) 91–100.
[14] R.G.M. van der Sman, S. van der Graaf, Diffuse interface model of surfactant adsorption onto flat and droplet interfaces, Rheol. Acta 46 (1) (2006) 3–11.
[15] M. El-Shahed, A. Salem, On the generalized Navier–Stokes equations, Appl. Math. Comput. 156 (2004) 287–293.
[16] E.B. Nauman, D.Q. He, Nonlinear diffusion and phase separation, Chem. Eng. Sci. 56 (2001) 1999–2018.
[17] H. Emmerich, Advances of and by phase-field modeling in condensed-matter physics, Adv. Phys. 57 (2008) 1–87.
[18] J. Lowengrub, L. Truskinovsky, Quasi-incompressible Cahn–Hilliard fluids and topological transitions, Proc. R. Soc. London A 454 (1998) 2617–2654.
[19] D.M. Anderson, G.B. McFadden, A.A. Wheeler, Diffuse interface methods in fluid mechanics, Annu. Rev. Fluid Mech. 30 (1998) 139–165.
[20] I. Tomashchuk, P. Sallamand, J.M. Jouvard, The modeling of dissimilar welding of immiscible materials by using a phase field method, Appl. Math. Comput. 219 (2013) 7103–7114.
[21] H. Liu, Y. Zhang, Phase-field modeling droplet dynamics with soluble surfactants, J. Comput. Phys. 229 (2010) 9166–9187.
[22] S. Komura, H. Kodama, Two-order-parameter model for an oil–water-surfactant system, Phys. Rev. E 55 (1997) 1722–1727.
[23] D. Jacqmin, Calculation of two-phase Navier–Stokes flows using phase-field modeling, J. Comput. Phys. 155 (1999) 96–127.
[24] H.A. Stone, Dynamics of drop deformation and breakup in viscous fluids, Annu. Rev. Fluid Mech. 26 (1994) 65–102.
[25] L.D. Landau, E.M. Lifshitz, Fluid Mechanics, Pergamon Press, New York, 1958.
[26] J.S. Kim, A continuous surface tension force formulation for diffuse-interface models, J. Comput. Phys. 204 (2005) 784–804.
[27] S. Khatri, A.-K. Tornberg, A numerical method for two-phase flows with insoluble surfactants, Comput. Fluids 49 (2011) 150–165.
[28] S. Velankar, H. Zhou, H. Jeon, C. Macosko, CFD evaluation of drop retraction methods for the measurement of interfacial tension of surfactant-laden drops, J. Colloid Interface Sci. 272 (1) (2004) 172–185.
[29] Y. Pawar, K. Stebe, Marangoni effects on drop deformations in an extensional flow: the role of surfactant physical chemistry. I. Insoluble surfactants, Phys. Fluids 8 (1996) 1738–1751.
[30] F. Harlow, J. Welch, Numerical calculation of time-dependent viscous incompressible flow of fluid with free surface, Phys. Fluids 8 (1965) 2182–2189.
[31] J.B. Bell, P. Colella, H.M. Glaz, A second-order projection method for the incompressible Navier–Stokes equations, J. Comput. Phys. 85 (1989) 257–283.
[32] U. Trottenberg, C. Oosterlee, A. Schüller, Multigrid, Academic press, UK, 2001.
[33] J.S. Kim, A numerical method for the Cahn–Hilliard equation with a variable mobility, Commun. Nonlinear Sci. Numer. Simul. 12 (2007) 1560–1571.
[34] J.S. Kim, H-O. Bae, An unconditionally stable adaptive mesh refinement for Cahn–Hilliard equation, J. Korean Phys. Soc. 53 (2008) 672–679.
[35] M. Francois, W. Shyy, Computations of drop dynamics with the immersed boundary method, Part 1: numerical algorithm and buoyancy-induced effect, Numer. Heat Transfer B 44 (2003) 101–118.